Amazon Coastal Squall Lines. Part I: Structure and Kinematics

MICHAEL GARSTANG, HAROLD L. MASSIE, JR.,* JEFFREY HALVERSON, STEVEN GRECO,† AND JOHN SCALA@

Department of Environmental Sciences, University of Virginia, Charlottesville, Virginia

(Manuscript received 22 June 1992, in final form 1 February 1993)

ABSTRACT

Mesoscale to synoptic-scale squall lines that form along the northeastern coast of South America as sea-breeze-induced instability lines and propagate through the Amazon Basin are investigated using data collected during the April–May 1987 Amazon Boundary Layer Experiment (ABLE 2B).

These systems, termed "Amazon coastal squall lines" (ACSL), have been noted by others, but details of the structure and evolution of the ACSL are limited. The present paper uses Geostationary Operational Environmental Satellite, radar, upper-air rawinsonde, and surface Portable Automated Mesonet data to describe the structure, dynamics, and life cycle of the ACSL. Twelve ACSL were sampled during ABLE 2B, and three cases are discussed in detail.

The ACSL are discontinuous lines of organized mesoscale cloud clusters that propagate across the central Amazon Basin at speeds of 50–60 km h^{-1}. The ACSL undergo six possible life cycle stages: coastal genesis, intensification, maturity, weakening, reintensification, and dissipation. Analysis also indicates that mesoscale clusters within the ACSL are composed of three distinct cloud components: a prestorm region that often contains towering cumulus, leading edge convection (LEC), and multiple, precipitating cloud layers in the trailing stratiform region (TSR).

Divergence and vertical velocity calculations indicate deep vertical ascent in the LEC and a region of midlevel convergence (≈500 mb) in the TSR. The latter midlevel convergence is associated with a weak updraft above 500 mb and an unsaturated downdraft below. Vertical motions in the TSR are an order of magnitude smaller than in the LEC.

Substantial shear in the low-level inflow occurs in all three case studies and, as suggested by model simulations, may play an important role in the longevity (24–48 h) of the ACSL. Profiles of equivalent potential temperature θ_e taken from the prestorm, leading edge convection and trailing stratiform regions demonstrate that the ACSL stabilize the troposphere in their wake and remove a tropospheric minimum of θ_e. It is hypothesized that the removal of this minimum is accomplished both by direct mixing via vertical motions in the LEC ("hot towers") and also through detrainment in the multiple-layered TSR. Part I describes the structure and kinematics of the ACSL, while Part II deals with the heat and moisture transports of these systems.

1. Introduction

Among the most important rain producers in the rain forests of the central Amazon Basin (CAB) of Brazil are mesoscale to synoptic-scale squall lines of coastal origin. These systems, which we will term "Amazon coastal squall lines" (ACSL), form along the northeastern coast of South America as a result of sea-breeze-induced convection. The ACSL often propagate away from the coast, reaching as far inland as Manaus, Brazil, in the CAB and, in some instances, the Andes 48 h after genesis (Kousky 1980; Molion 1987).

Both Kousky (1980) and Molion (1987) have presented sequences of satellite images that illustrate the coastal genesis and inland propagation of a squall line in the Amazon Basin. Molion (1987) found that these lines of instability, or squall lines, may be over 1000 km long and propagate across the Amazon Basin with average speeds of 10° longitude per day or 45–55 km h^{-1}. Kousky and Molion (1981) and Molion (1987) have suggested that the diurnal cycle and propagation characteristics associated with these squall lines may explain the relatively smaller precipitation values observed in the lower Amazon compared to the precipitation maximum in the central and western Amazon.

More recently, Greco et al. (1990) used data collected during the wet season Amazon Boundary Layer Experiment (ABLE 2B) in April–May 1987 to investigate the ACSL, termed "coastal occurring systems" (COS) in their work. Greco et al. (1990) found that

* Also affiliated with Air Weather Service Headquarters, Scott Air Force Base, Illinois.

† Current affiliation: SM Systems and Research Corporation, Washington, D.C.

@ Also affiliated with Severe Storms Branch, NASA/Goddard Space Flight Center, Greenbelt, Maryland.

Corresponding author address: Prof. Michael Garstang, Department of Environmental Sciences, Clark Hall, University of Virginia, Charlottesville, VA 22903.

these COS are generally 1000–2000 km long but may attain a maximum length up to 3500 km. In addition, they estimated that the COS propagate across the basin at speeds of 50–60 km h^{-1} and were observed to last 24–48 h. Similar results were reported by Cohen et al. (1989) in a study of "propagating squall lines" using hourly satellite imagery between 1979 and 1986. Silva Dias and Ferreira (1992) use a linear spectral model to study the dynamics of Amazon squall lines. An important finding of Greco et al. (1990) was that the 12 COS occurring during the ABLE 2B (1 April–15 May 1987) produced 40% of the experiment rainfall. Cohen et al. (1989) found that these types of squall lines are most common in the CAB between April and August.

The studies cited above provide only a qualitative description of the ACSL. Detailed investigations of the structure, flow field, and energetics of the ACSL have been very limited (Scala et al. 1990) due mainly to the paucity of data in the relatively harsh environment of the Amazon rain forest. The main goal of this paper is to use data collected from satellites and a mesoscale network of surface and upper-air stations employed in the CAB during ABLE 2B to investigate the structure and kinematics of the ACSL on the mesoscale and convective scale. An additional goal is to compare the ACSL with other tropical and nontropical squall lines. Although satellite imagery and preliminary analyses suggest similarities with the West African (Chalon et al. 1988; Chong et al. 1987), tropical Atlantic (Barnes and Sieckman 1984), Venezuelan (Betts et al. 1976), and even the United States midlatitude (Ogura and Liou 1980) squall lines, a more quantitative assessment is needed and will be presented in this work.

This paper, which is the first of a two-part study on the ACSL, will document the life cycle and cloud components (sections 3a and 3b), and both the kinematic and thermodynamic structure (sections 3c and 3d), of the ACSL as they propagate through the CAB. Important similarities and differences between the structure of the ACSL and other tropical and nontropical squall lines will be discussed in sections 3b and 3c. Section 3d will also detail important implications of the ACSL cloud structure on the larger-scale dynamics of the CAB. Part II of this study will deal with the heat transports associated with the ACSL in the Amazon Basin. In particular, the focus will be upon the contributions of the ACSL heat transports to the total heat export from the tropics and the relative importance of the heat transport produced by the stratiform regions of the ACSL.

2. Data

The National Aeronautics and Space Administration (NASA), in cooperation with the Brazilian Instituto Nacional de Pesquisas Espaciases (INPE) and Instituto Nacional de Pesquisas da Amazonia (INPA), conducted the wet season ABLE 2B during 1 April–15 May 1987. A detailed description of the ABLE 2B can be found in Harriss et al. (1990) and Garstang et al. (1990). ABLE 2B, as part of NASA's Global Tropospheric Experiment (GTE), was primarily an atmospheric chemistry experiment. However, ABLE 2B also included an extensive meteorological component that enabled the study of atmospheric motions ranging from the turbulent to the planetary scale.

The ABLE 2B meteorological networks provided the focus for mesoscale through synoptic-scale sampling, which was necessary for the study of convective systems over the vast, relatively inaccessible Amazon rain forests. The measurement systems operated during ABLE 2B included both ground- and space-based platforms.

Rawinsondes were released nearly simultaneously every 3 h at the three corner stations of a 1000-km^2 mesoscale triangle network located in the CAB (Fig. 1). Procedures for reducing and adjusting these data are described below. After data reduction, the soundings provided horizontal wind velocity, temperature, and mixing ratio from the surface to 100 mb.

Portable Automated Mesonet (PAM) stations, the Geostationary Operational Environmental Satellite (GOES) platform, and a 3-cm radar acquisition system all continuously monitored the atmosphere in the network triangle and the CAB. These measurements provided the data used to define and partition the ACSL into distinct cloud components. Four single-level PAM stations (Fig. 1), located 5 m above the rain forest canopy on 40-m towers, measured horizontal wind velocity, temperature, humidity, pressure, and precipitation within the mesoscale network. The PAM measurements, obtained at a frequency of 1 Hz and stored as 1-min averages, were transmitted via satellite to the National Center for Atmospheric Research (NCAR) for processing and storage.

The GOES data consisted of visible and infrared (IR) images obtained via a Digital Weather Image Processing System (DWIPS) operated at the ABLE 2B operations center at Eduardo Gomes Airport (EGA) in Manaus. The GOES images were used to analyze cloud conditions over the mesoscale triangle and to document the movement of synoptic disturbances. An ACSL life cycle taxonomy is derived from images obtained over the entire experiment.

A 3-cm radar located at EGA provided constant-altitude plan position indicator (CAPPI) scans of the mesoscale triangle at 5-min intervals. Signal attenuation severely degraded the CAPPI data during heavy precipitation, thereby limiting the radar's usefulness for making accurate estimates of rainfall rates and aerial coverage.

The mesoscale rawinsonde data used in this study were checked against climatology and rawinsonde profiles measured coincidently by a six-station basin-scale network (Fig. 1), which was also part of the ABLE 2B experiment. This comparison revealed pronounced

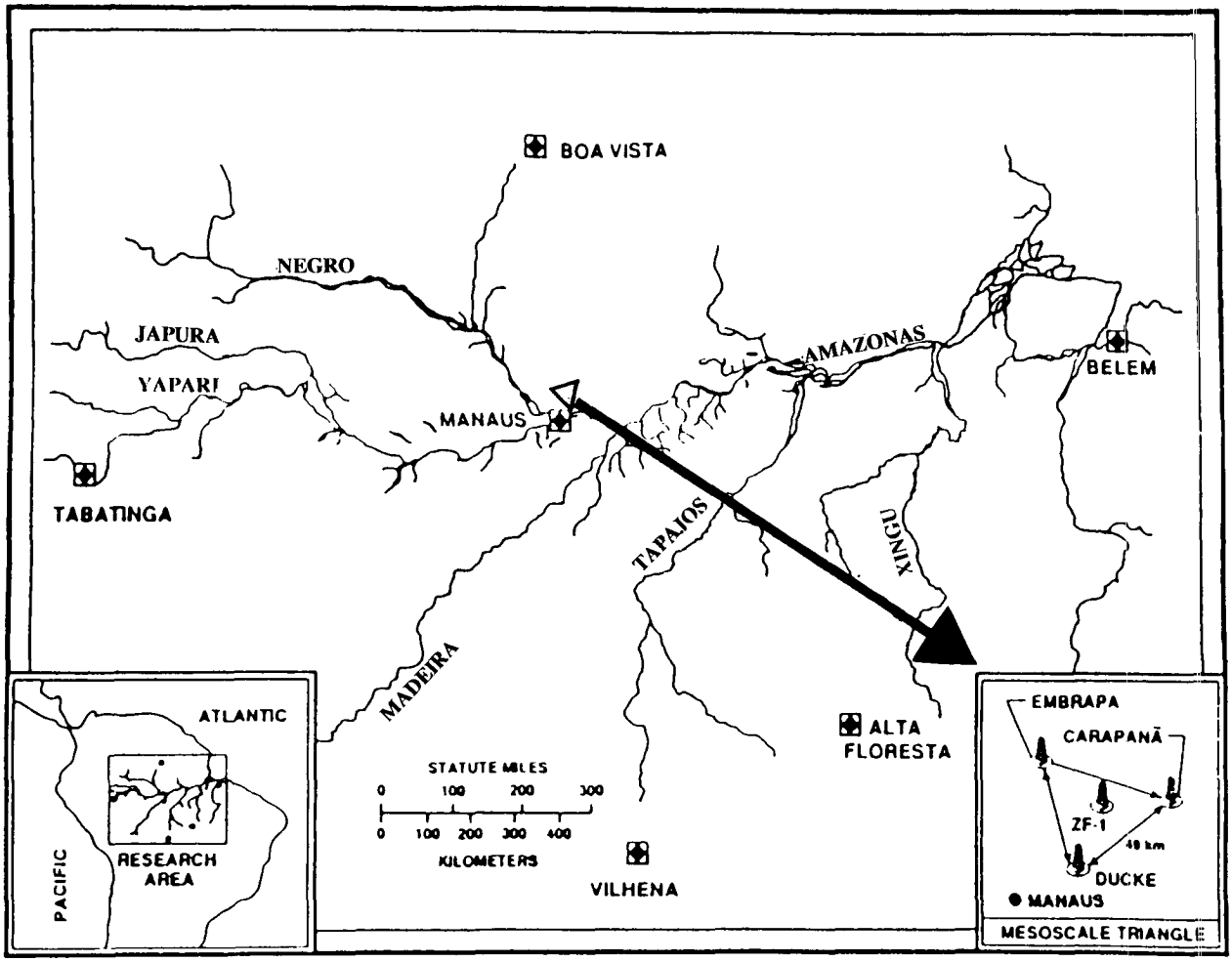

FIG. 1. Location and design of the meteorological network used from 1 April to 15 May 1987 during ABLE 2B. Rawinsonde and PAM towers were located on the corners of the mesoscale triangle (see inset) with a fourth PAM at the center. A large-scale network of rawinsondes covering the basin is marked with diamond in the square.

pressure offset problems in the mesoscale triangle soundings that were ultimately traced to bad instrument calibrations by the rawinsonde manufacturer.

A least-squares procedure based on the mean basin-scale temperature profile was used to develop a procedure for adjusting and editing the mesoscale soundings. After the pressure offset was determined, temperatures were reassigned to adjusted pressure levels. Geopotential, mixing ratio, and wind velocity were then recalculated at 25-mb intervals from the surface to 100 mb. The wind calculations employed a smoothed azimuth, elevation, and balloon ascent rate derived from a three-point moving average (Davis 1986) to reduce noise introduced by antenna errors.

Some soundings launched during thunderstorms experienced data losses due to icing problems. Usually these soundings terminated near the freezing level (located at 600 mb). These weather-related problems and the difficulties associated with sampling a phenomena with pronounced mesoscale spatial and temporal variability prevented us from making calculations for several strong ACSL that passed through the mesoscale network. The cases selected for study either had no problems or contained data deficiencies that were easily handled by the above procedures.

Divergence for the mesoscale triangle is computed from the line integral of the wind components normal to each leg (Gamache and Houze 1982). Divergence is calculated from 1000 to 100 mb in 25-mb intervals. The vertical velocity at each pressure level is determined first from the vertically integrated divergence and then adjusted by O'Brien's (1970) method, which forces the vertical velocity to zero at the surface and at the highest level (100 mb).

This procedure gives results that compare well with physically realistic estimates of vertical motion from adiabatic and isentropic methods (Haltiner and Martin 1957). Gamache and Houze (1982) obtained accept-

able results by applying these procedures to tropical squall lines.

3. Results

a. Definition of the ACSL life cycle

Analysis of both GOES imagery and PAM surface data have shown that 12 ACSL were detected in the CAB during the ABLE 2B wet season (Greco et al. 1990). These large and generally linear mesoscale to synoptic-scale systems form along the northeastern coast of South America in midafternoon and move across the Amazon Basin, usually from northeast to southwest, at an average speed of 50–60 km h^{-1}. At maturation, ACSL are usually 1000–2000 km long and 100–300 km wide. The ACSL often last between 24 and 48 h, reaching the ABLE 2B experiment region in the central Amazon Basin 20–24 h after formation along the coast. Figure 2, taken from Greco et al. (1990), shows the composite hourly cloud cover percentages from the GOES-West brightness temperatures less than 240 K for the 12 ACSL days. The development of the squall or cloud line along the coast by 2200 UTC (1800 LST, Fig. 2a) is clearly shown. The existence, at the same time, of another cloud line to the west already in the CAB should be noted. This is the previous day's ACSL. The propagation of the ACSL from near the coast at 2000 UTC to the CAB 18 h later (1600 UTC, Fig. 2d) is graphically shown.

Greco et al. (1990) showed that these massive, long-lived convective systems accounted for at least 40% of the total rainfall in the mesoscale network during ABLE 2B. Their importance to the water budget of the Amazon Basin makes it necessary to undertake a detailed study of their life cycle and the evolution of the flow field and kinematic structure.

The GOES visible and IR images collected during ABLE 2B indicate that patterns, sizes, intensities of clouds, and rainfall can change dramatically during the lifetime of an ACSL. The GOES images from April and May 1987 have been studied to define an ACSL life cycle of six possible stages.

1) COASTAL GENESIS

During coastal genesis, the first thunderstorm cells form during the afternoon in the sea-breeze convergence zone along the northeastern coast of South America. The number and size of the cells increases with time, followed by selective merging into thunderstorm clusters with shared anvils.

2) INTENSIFICATION

During late afternoon and evening, merging continues as small clusters of thunderstorms merge to form

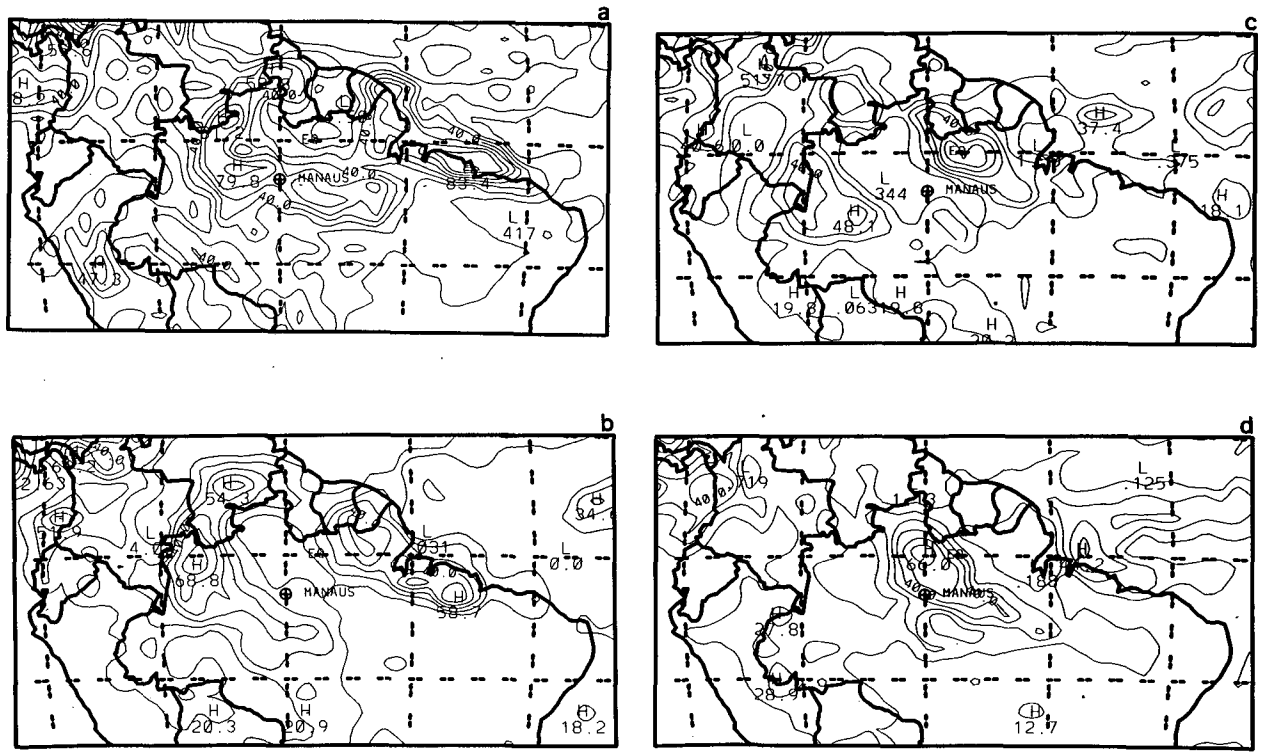

FIG. 2. Composite hourly cloud cover percentage for GOES-West brightness temperature less than 240 K for 12 ACSL days during ABLE 2B. Times shown are (a) 2200 UTC, (b) 0400 UTC, (c) 1000 UTC, and (d) 1600 UTC.

larger clusters, generally oriented from northwest to southeast in a quasi-linear pattern parallel to the coastline of northeastern Brazil. Figure 3a illustrates the intensification of clustering of the sea-breeze-forced convection at 0330 UTC 26 April 1987. The strongest clusters containing intensifying convective elements and anvils are resolved by black tones on GOES images using the MB enhancement technique (Carlson 1981). The strong clusters have sharp boundaries and cloud-top temperatures colder than 212.8 K, indicating a height of approximately 13–14 km. Patches of white within the mesoscale clusters indicate cumulonimbi with cloud-top temperatures less than 192.8 K and heights of 16–17 km.

By early morning (1000 UTC, Fig. 3b), the disturbance has increased in length, and at this time is best described as an undulating arc of clusters that vary in their intensity and size. During the 6.5-h period between 0330 and 1000 UTC, the largest convective cluster located at *A* (0330 UTC, Fig. 3a) has weakened and a warmer, midlevel cloud shield has spread horizontally, while a new concentration of cumulonimbi has formed and matured at *B* (1000 UTC, Fig. 3b).

3) MATURATION

During this stage, the entire system achieves maximum length and width. At maturation, ACSL can reach a total length of over 3000 km and are often a dominant synoptic-scale cloud feature over a third of the tropics appearing on GOES full-disk images (Molion 1987). This is illustrated in Fig. 3c, which shows the ACSL of 1700 UTC 26 April as it approaches the mesoscale network. This ACSL was approximately 3500 km long at the time of strongest intensity, although only 1000 km may have contained active convection. The ACSL is not a continuous line of cells but rather a highly discontinuous line or arc of discrete clusters of cells,

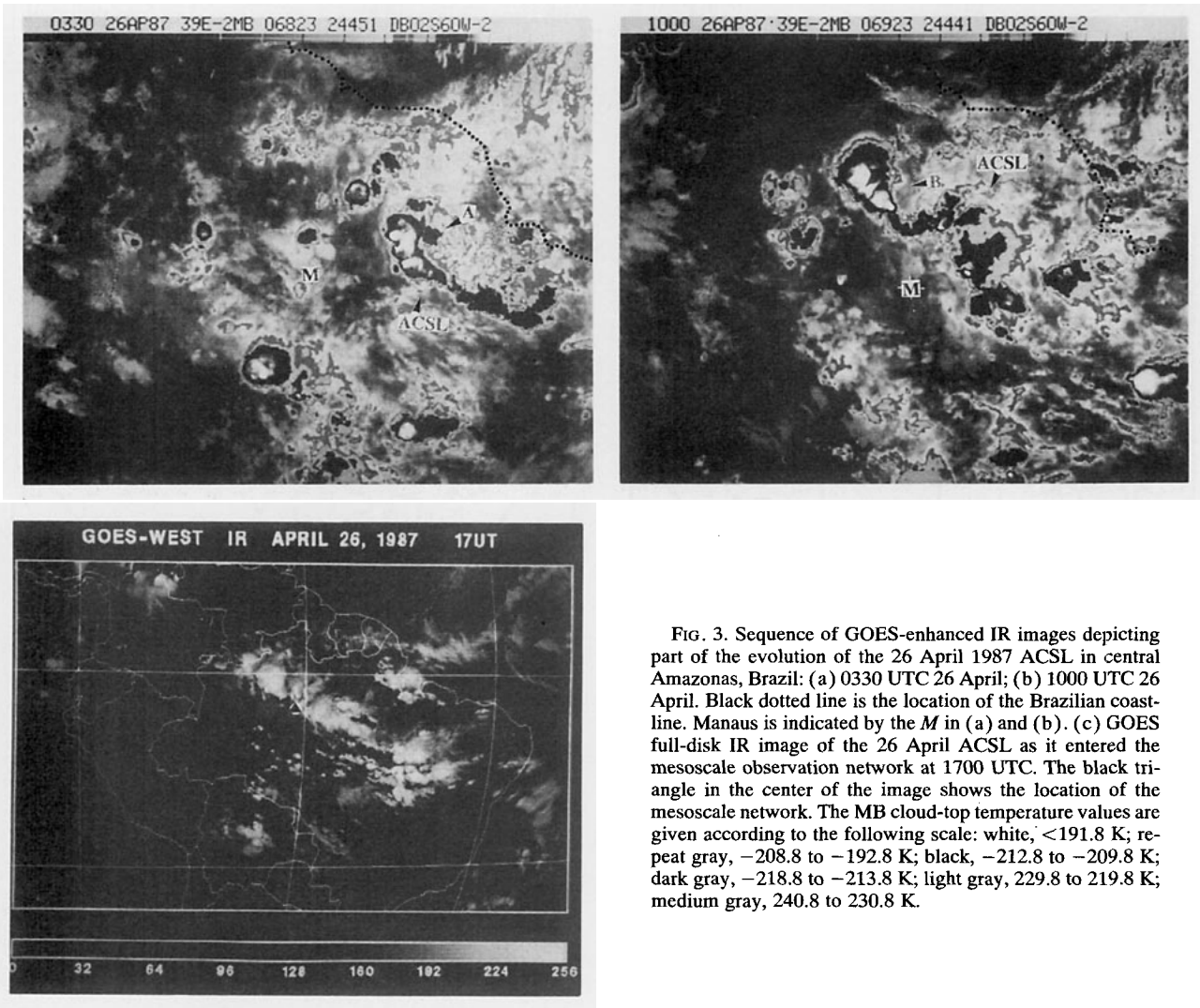

FIG. 3. Sequence of GOES-enhanced IR images depicting part of the evolution of the 26 April 1987 ACSL in central Amazonas, Brazil: (a) 0330 UTC 26 April; (b) 1000 UTC 26 April. Black dotted line is the location of the Brazilian coastline. Manaus is indicated by the *M* in (a) and (b). (c) GOES full-disk IR image of the 26 April ACSL as it entered the mesoscale observation network at 1700 UTC. The black triangle in the center of the image shows the location of the mesoscale network. The MB cloud-top temperature values are given according to the following scale: white, <191.8 K; repeat gray, −208.8 to −192.8 K; black, −212.8 to −209.8 K; dark gray, −218.8 to −213.8 K; light gray, 229.8 to 219.8 K; medium gray, 240.8 to 230.8 K.

organized on the mesoscale. Typically only 30%–40% of the leading edge consists of active deep convection. In this image, the formation of a new ACSL is also evident along the northeast coast of Brazil.

4) WEAKENING

The clusters diminish in size, and the definition of the outer edges becomes ragged on the Mb-enhanced images. Areas previously shown in black on the Mb images change to dark (219–214 K) and light gray (230–220 K), indicating warmer cloud-top temperatures and weaker thunderstorms. The width of the ACSL decreases to 100–200 km. Some ACSL experience a slowing in forward speed and a tendency to weaken as they approach the confluence of large river systems in the vicinity of Manaus. The PAM-derived rainfall, corroborated with a network of additional gauges located along the Rio Amazonas at Manaus, show a 50% reduction in project total rainfall for synoptic systems in the vicinity of the river.

5) REGENERATION

Following a period of weakening, several systems regenerate as they propagate to the west of Manaus during the period of maximum diurnal heating. During regeneration, an enlargement of the black areas with a sharp outer definition on the Mb images indicates thunderstorm clusters that are growing and intensifying. The system's synoptic-scale features become better defined on the IR images.

6) DISSIPATION

After a period of weakening, the individual clusters become more ragged and ultimately disappear. The system loses its synoptic-scale definition on the IR images.

The above description of the ACSL life cycle is similar to taxonomies developed for other tropical squall-line-type mesoscale convective systems (e.g., Houze 1977; Frank 1978; Leary and Houze 1979). This present taxonomy, however, defines the life cycle of a much larger mesoscale to synoptic-scale convective disturbance. We have classified three ACSL as they passed through the mesoscale network according to the above taxonomy: the ACSL on 26 April 1987 is classified as weakening, the one on 1 May 1987 as mature, and the one on 6 May 1987 as a regenerating system.

b. ACSL cloud and rainfall components

A combination of radar, satellite, and PAM data is used to identify distinct types of cloud components within the individual mesoscale cloud clusters. The ACSL have a convective and stratiform structure similar to the design of Gamache and Houze (1982) and satisfy Zipser's (1977) criteria for a tropical squall system. The three primary cloud components composing ACSL are the following: a prestorm region ahead of the squall front that often contains developing cumulus towers; leading edge convection (LEC); and widespread layers of precipitating midlevel and anvil cloud within the trailing stratiform region (TSR).

Figure 4 presents an enlarged, enhanced GOES IR image of the central Amazon Basin for 1700 UTC 26 April 1987. The discontinuous, linear arrangement of cloud clusters is clearly visible. The coldest cloud tops marked in black in the enhancement are less than 178 K. Individual cluster elements are composed of deep cumulonimbus along the leading edge. A shield of warmer anvil cloud surrounds these cells and extends to the rear of the clusters.

Analysis of 5-min CAPPI radar scans with 2-km resolution was used in conjunction with the satellite images to identify cloud components. An example is given in the sequence of radar images for 1702 and 1730 UTC 26 April 1987 (Figs. 5a and 5b). A sharp reflectivity gradient delineates the leading edge of the convection as the ACSL propagates across the surface network triangle (stippled region). An area of lower reflectivity, possibly indicating the "transition" region (Smull and Houze 1987), separates the stronger activity within the trailing stratiform region from the leading convection. New convective elements are observed to form ahead of the leading edge of the main squall line at 1730 UTC (Fig. 5b).

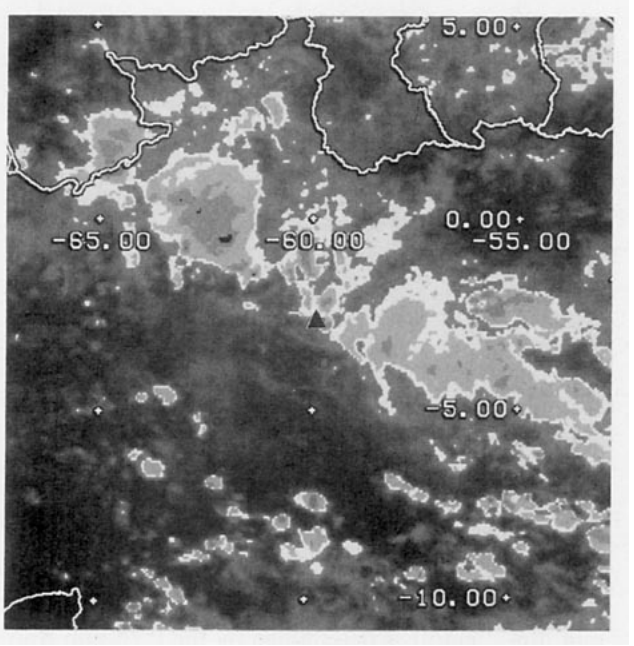

FIG. 4. GOES-enhanced IR image of the central Amazon Basin for 1700 UTC 26 April 1987. Coldest cloud tops marked by black are less than 198 K. Numbers on the figure are latitude and longitude. Location of the mesoscale network is indicated by the triangle (2.7°S, 60°W).

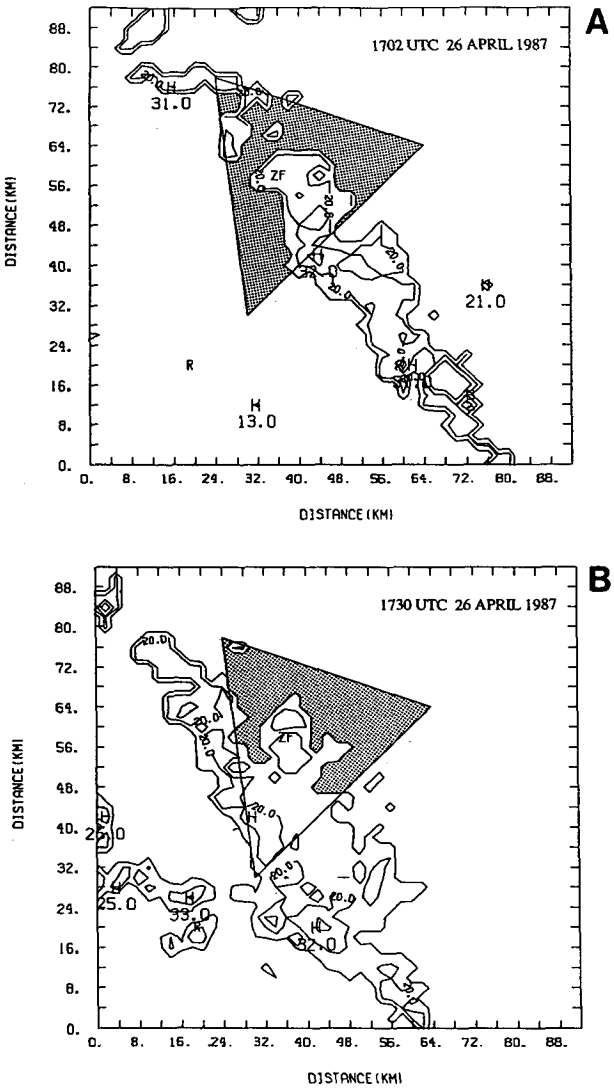

FIG. 5. Sequence of CAPPI radar images at 2-km resolution for (a) 1702 UTC 26 April 1987 and (b) 1730 UTC 26 April 1987. The ABLE surface network triangle is stippled. The letter *R* marks the location of the radar.

Important to the identification of cloud components is an analysis of the high-frequency PAM data that is used to delineate the three ACSL components. The 1-min-averaged values of T, q, θ_e, and wind speed clearly identify the passing of the squall front. Rainfall rates measured by the tipping-bucket raingage mounted on the PAM platform, 5 m above the canopy, are employed to determine the transition from the deep convective stage to the anvil stage using 0.25 mm min^{-1} as a cutoff from convective to stratiform rain. The 0.25 mm min^{-1} cutoff is determined by the 0.25-mm resolution of the tipping-bucket raingage.

Figure 6 shows the time series of PAM observations recorded at Embrapa on 26 April 1987. The arrival of the gust front is clearly noted between 1630 and 1700 UTC. The response of surface variables to the passage of the gust front at Ducke, Embrapa, Carapaña, and ZF 1 on 26 April 1987 and 6 May 1987 are summarized in Table 1. Results for 1 May 1987 are not shown, because lightning disrupted the PAM network during ACSL passage. There are large differences among the four PAM stations in rainfall rate and changes of T, q, P, and θ_e, especially on 6 May 1987. These differences reflect the spatial discontinuity of the ACSL on the mesoscale.

c. *Squall-line kinematics and dynamics*

In this section, analysis of the mesoscale network PAM and rawinsonde data is used to show the cross-sectional (normal to direction of storm propagation) structure and characteristics of the 1 May 1987 ACSL. We have chosen to emphasize details of the 1 May case because of the completeness of the rawinsonde coverage for both the LEC and TSR components of this squall line. Observations taken from the mesoscale triangle, however, did capture the TSR components of the 26 April and 6 May systems, and we compare the general kinematic structure of this region among the three squall systems.

The 1 May ACSL formed during the midafternoon of 30 April 1987 as a line of numerous small convective clusters located along the northeast coast of Brazil. By late afternoon, the clusters had grown rapidly and merged to form a synoptic arc-shaped ACSL. By early evening, the arc acquired a more linear appearance as it propagated toward the southwest at 33 km h^{-1} (Fig. 7). A group of smaller mesoscale clusters formed 250 km ahead of the ACSL leading edge. These clusters produced heavy rain in the northern part of the mesoscale triangle 6 h prior to the arrival of the ACSL at 1200 UTC 1 May.

Mass divergence is calculated for the mesoscale network volume using the near-simultaneous rawinsonde launches at the triangle vertices (Ducke, Embrapa, Carapaña). A simple line integral method is used. Vertical profiles of the divergence values calculated for the LEC (1200 UTC) and TSR (1800 UTC) components of the 1 May ACSL are shown in Fig. 8. The LEC profile is characterized by a pronounced vertical couplet of convergence (-1.6×10^{-4} s^{-1}) between 600 and 700 mb and divergence (1.8×10^{-4} s^{-1}) located between 300 and 500 mb within the deep convective region. Vertical profiles of vertical p velocity for the LEC and TSR components resulting from the divergence profiles of Fig. 8 are shown in Fig. 9. The divergence couplet is associated with deep upward motion in the LEC with a peak of more than 40 μb s^{-1} near 550 mb. Figure 10 shows the LEC (1200 UTC) and TSR (1800 UTC) composite vertical profiles of temperature and dewpoint temperature for the triangle. The "composite" sounding is constructed from the three soundings at the corners of the mesoscale triangle at each time. Note

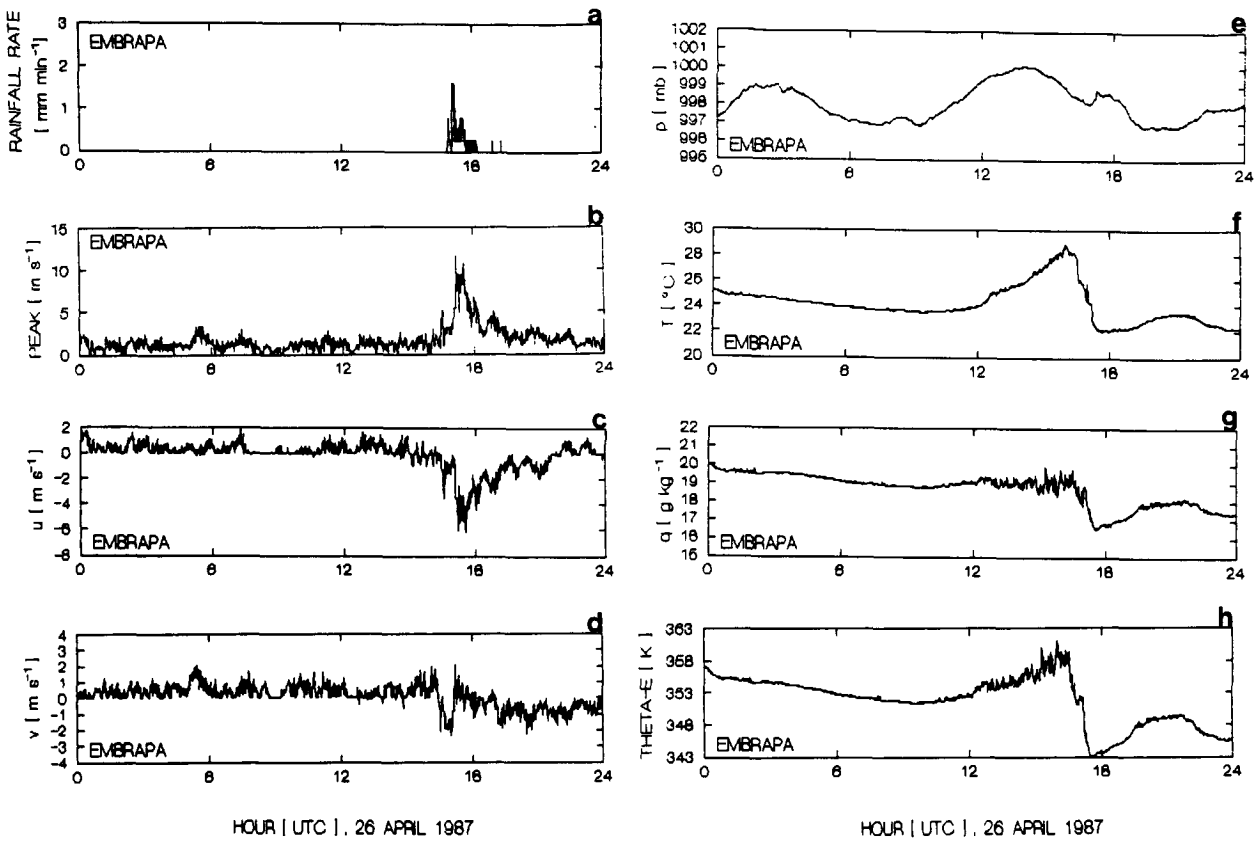

FIG. 6. Time series of PAM-measured surface variables during passage of the 26 April 1987 ACSL at Embrapa at the northwest corner of the mesoscale triangle. One-minute averages are shown for (a) rainfall rate (mm min^{-1}), (b) peak wind gust (m s^{-1}), (c) u wind component (m s^{-1}), (d) v wind component (m s^{-1}), (e) pressure (hPa), (f) temperature (K), (g) mixing ratio (g kg^{-1}), and (h) equivalent potential temperature θ_e (K).

that the deep convective ascent coincides with saturated conditions to a level of 500 mb. It is likely that the 1200 UTC sounding ascended through and directly sampled a portion of deep convective towers within the LEC.

Six hours following the storm passage, the divergence profile of the TSR is relatively weak throughout the depth of the troposphere and includes a layer of divergence that extends from 800 mb to the surface. Peak downward motion is indicated at 800 mb in the TSR, accompanied by progressive warming and drying of the layer (Fig. 10). Higher in the atmosphere, weak ascent (5–10 $\mu b\ s^{-1}$) is found between 600 mb and the tropopause. The peak in the upward motion coincides with the upper portion of a midlevel saturated (cloud) layer seen at 1800 UTC in the thermodynamic profiles. The 1800 UTC sounding indicates that the boundary layer is recovering from the convective disturbance. (Note the warming and moistening in the surface layer between 1200 and 1800 UTC.) However, the formation of a warm, dry subsidence-induced inversion in the low levels combined with a distinct region of warming above 500 mb suppresses new deep convective activity in the wake of the squall line.

The vertical p-velocity values are consistent with the findings of Gamache and Houze (1982), who have shown that upward vertical motion is an order of magnitude larger in the convective region than in the stratiform region. The double-updraft structure, composed of a concentrated core of rising motion in the leading convective elements and weaker ascent in the trailing stratiform cloud region, is a feature that characterizes many mesoscale convective systems in the tropics—including systems observed during Convection Profonde Tropicale (COPT81) (Chalon et al. 1988), the Australian Monsoon Experiment (AMEX) (Frank and McBride 1989), the Global Atmospheric Research Program (GARP) Atlantic Tropical Experiment (GATE) (Gamache and Houze 1982), and the Winter Monsoon Experiment (WMONEX, Johnson and Priegnitz 1981)—and in the midlatitudes (Gallus and Johnson 1991).

Figure 11 presents a comparison of vertical p-velocity calculations for each of the three TSR on 26 April,

TABLE 1. Summary of changes in surface values of temperature (ΔT), humidity (Δq), equivalent potential temperature ($\Delta\theta_e$), and pressure (Δp) observed at the four PAM locations with the passage of the squall line on (a) 26 April and (b) 6 May. Also presented are peak wind gusts, maximum rain rate, and both total amount and duration of rainfall.

	Ducke	Carapaña	Embrapa	ZF1
(a) 26 April 1987				
ΔT (°C)	−6	−6.5	−7.0	−6.0
Δq (g kg^{-1})	−3.7	−2.1	−2.5	−2.6
$\Delta\theta_e$ (K)	−17.0	−11.0	−16.0	—
ΔP (hPa)	+0.7	+0.8	+0.9	+0.9
Peak gust (m s^{-1})	13	9	12	13
Maximum rain rate (mm min^{-1})	0.25	1.5	1.7	1
Total rainfall (mm)	1	34	33	16
Total duration of rainfall (h)	0.25	2.5	3.0	2.0
(b) 6 May 1987				
ΔT (°C)	−7.0	−3.5	−5.5	−4.0
Δq (g kg^{-1})	−1.5	No change	−1.5	No change
$\Delta\theta_e$ (K)	−7.0	−5.5	−9.0	—
ΔP (hPa)	+0.6	No change	+0.4	No change
Peak gust (m s^{-1})	7.5	6.5	15.0	8
Maximum rain rate (mm min^{-1})	1.3	0.8	0.5	0.3
Total rainfall (mm)	6	15	2	1
Total duration of rainfall (h)	1.5	8.0	6.0	1.0

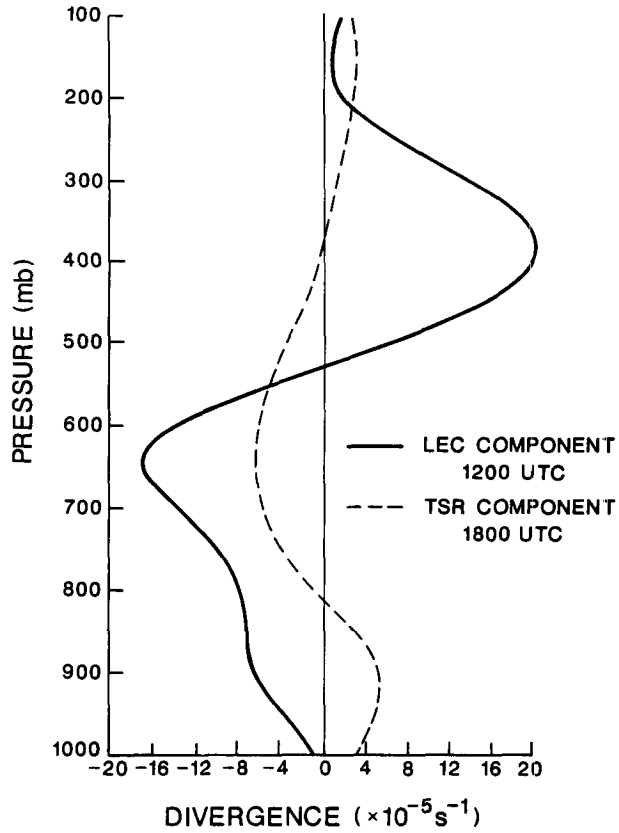

FIG. 8. Vertical profiles of mass divergence on 1 May 1987. Solid curve depicts the squall line LEC component at 1200 UTC. Dashed curve is the TSR component at 1800 UTC. Values are in units of 10^{-5} s^{-1}.

1 May, and 6 May. In general, weak ascent occupies the upper portion of the troposphere (above 500 mb) in each of the three TSR, with descending motion in the lower layers. The weakest motions are those associated with the 6 May regenerating case. The upward motion in the weakening 26 April system occupies nearly the entire troposphere (except for a shallow subsidence layer below 850 mb), and the magnitude of the motions in this deep layer are nearly the same as in the mature system. These findings may suggest that ascent in the trailing anvil plays a more important role during the late stages of the ACSL life cycle. However, since our analysis compares the life cycle stages of individual systems on different days, the observed differences in velocity structure might also reflect variability in the large-scale tropospheric conditions that in turn influence the intensity and organization of the squall-line circulations.

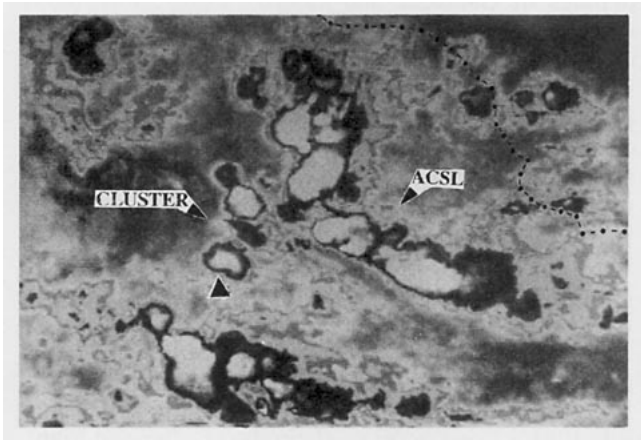

FIG. 7. GOES MB-enhanced infrared image of the 1 May 1987 ACSL at 0230 UTC as it propagated westward across the mesoscale triangle (marked by the triangle). The coastline of Brazil is located along the dash–dot line.

The line-normal component of the storm-relative flow $\mathbf{V}_R$ (defined below) is calculated for the three ACSL systems. These calculations use a storm coordinate system defined by an x' axis oriented orthogonally to the leading edge of each squall line (Fig. 12). The angle α between the storm coordinate x' axis and the x axis in meteorological coordinates is used to derive a line-normal wind component $\mathbf{V}_N$, where $\mathbf{V}_N$ is one of four wind vectors or wind components defined as follows:

$\mathbf{V}_E$—measured wind vector
$\mathbf{V}_N$—line-normal wind component

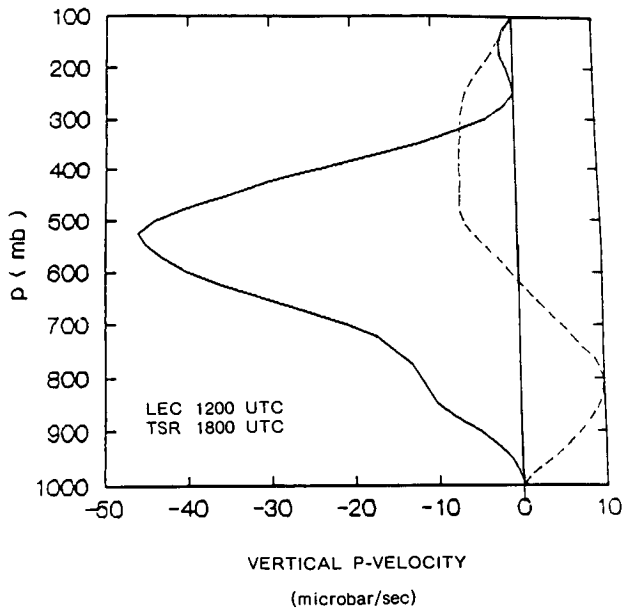

FIG. 9. Vertical profiles of vertical p velocity (μb s^{-1}) for the 1 May 1987 ACSL. Solid curve depicts the squall line LEC component at 1200 UTC; dashed curve is the TSR component at 1800 UTC.

$\mathbf{V}_S$—storm translational velocity
$\mathbf{V}_R$—storm-relative winds—$\mathbf{V}_N - \mathbf{V}_S$

Representative measured wind vectors $\mathbf{V}_E$ are shown in Fig. 13 for the region just ahead of the LEC (1500 UTC 26 April and 6 May) and in the LEC (1200 UTC 1 May).

For the three cases of 26 April, 1 May, and 6 May, the angle α is 50°, 60°, and 45°, and the storm speeds $\mathbf{V}_S$ are 6 m s^{-1} (22 km h^{-1}), 9 m s^{-1} (32 km h^{-1}), and 10 m s^{-1} (36 km h^{-1}), respectively. The storm-relative flow $\mathbf{V}_R$ profiles for all three cases are shown in Fig. 14. All three cases show a pronounced shear in the lowest levels. This front-to-rear low-level inflow results from storm motion, which in turn is a consequence of a low-level wind maximum is shown in Fig. 13. This maximum ranges in intensity from 8 to 15 m s^{-1}. The wind maxima are located in the 650–850-mb layer and are observed to accompany the squall lines as they propagate through the ABLE 2B surface network. A similar wind maximum, the African easterly jet, is associated with West African squall lines investigated during COPT81 (Chong et al. 1987). The observed relative flow profiles in their study are very similar to those identified for Amazon systems.

The low-level shear associated with the three ACSL also suggests a mechanism for their observed longevity. Rotunno et al. (1988) have demonstrated that the vigorous, sustained lifting along the squall leading edge is maintained by a balance between counterrotating circulations generated by the shear in the outflow cold pools and the opposing low-level relative inflow. Thorpe et al. (1982) have proposed that strong low-level shear relative to the storm prevents the outflow boundary from propagating away from the storm leading edge and thus cutting off the storm's available supply of moist boundary-layer air. The 2D version of the Goddard cumulus ensemble (GCE) model (Soong and Tao 1980; Soong and Ogura 1980; Tao and Soong 1986; Tao and Simpson 1989, 1992; Tao et al. 1991; Simpson and Tao 1992) was used to simulate the dynamics of Amazon systems (Garstang et al. 1990; Scala et al. 1990; Pickering et al. 1991, 1992). Simulation of the 26 April and 6 May convective events revealed that the storm outflows remained close to the leading edge convection and indicated the potential for convective demise when the updraft and downdraft interface sloped too far upshear. This action initiated a forward surge of the outflow boundary that terminated the influx of high-θ_e air into the developing cells. A convective balance between the low-level shear and storm-induced outflows is likely required for the long-lived storms

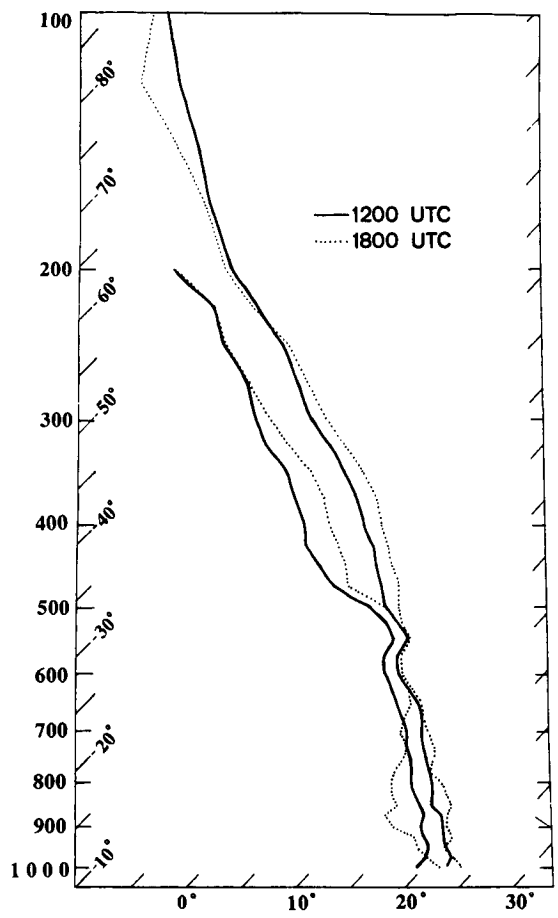

FIG. 10. Vertical profiles of sounding-derived temperature and dewpoint for the 1 May 1987 ACSL in standard skew T–log$p$ format. Mesoscale triangle composite soundings (from the three corners) are used for LEC (1200 UTC, solid curve) and TSR (1800 UTC, dashed curve) observations.

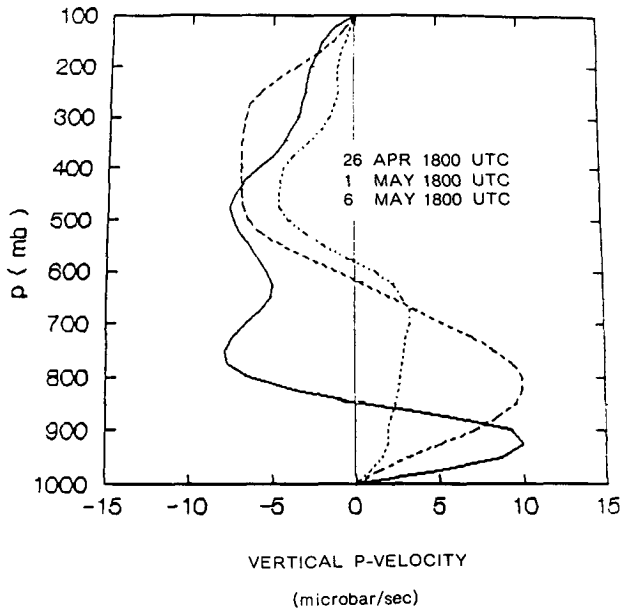

FIG. 11. Vertical profiles of vertical p velocity for the TSR of the 26 April (solid curve), 1 May (dashed curve), and 6 May (dash–dot curve) 1987 squall lines.

observed over the Amazon Basin (Rotunno et al. 1988).

A distinct minimum in relative flow into the front of the storm is located at 2.5 km for the three Amazon systems. If the relative flow calculation is extrapolated to the rear of the 6 May convective region, there is evidence of weak rear inflow located at 3 km. This inflow can provide a source of momentum and potentially low-θ_e air to drive convective-scale downdrafts. Low-θ_e air also enters the front of the three squall cases at midlevels between 4 and 8 km. While the trajectories of these relative flow paths within the storm system are not easily deduced from observations, model simulations (Scala et al. 1990; Pickering et al. 1992) suggest that parcels are entrained into the updraft cores and also become incorporated into convective scale downdrafts through mixing processes in the storm midlevels.

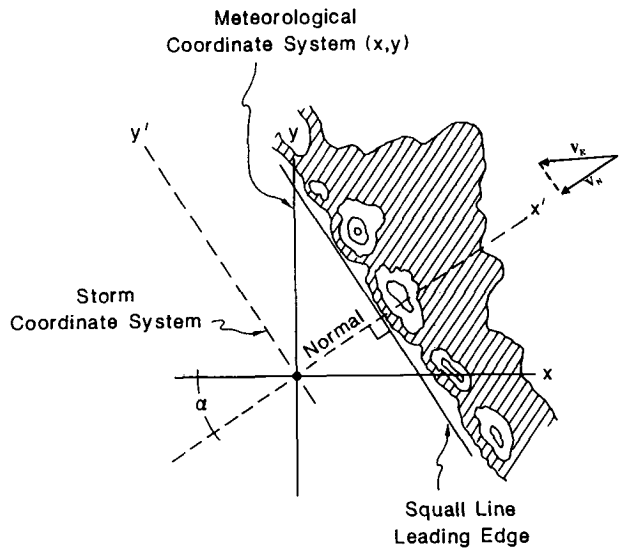

FIG. 12. Coordinate system used to derive the relative flow line-normal component for the 1 May 1987 ACSL.

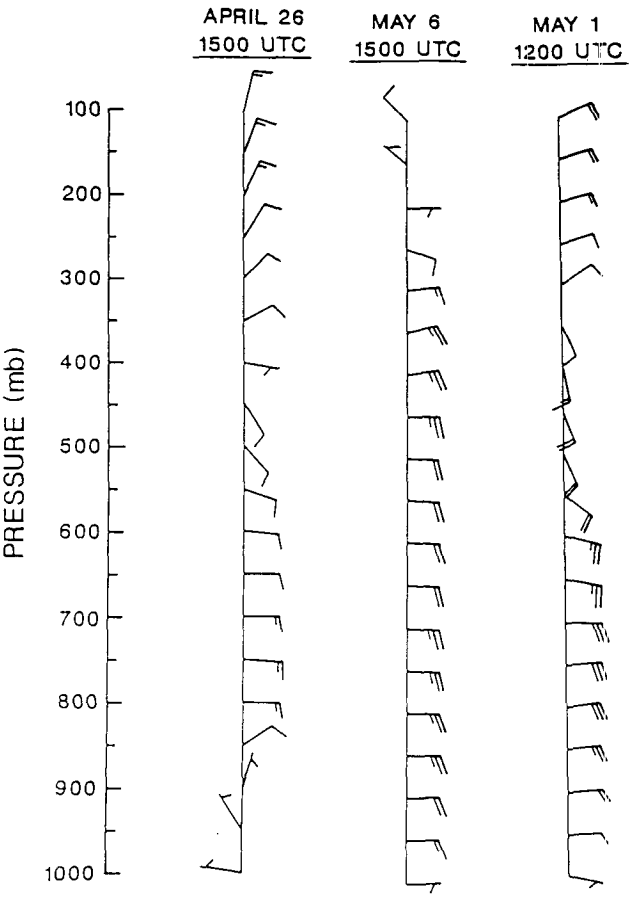

FIG. 13. Profiles of wind velocity for three ACSL prestorm, 26 April (1500 UTC) and 6 May 1987 (1500 UTC) and LEC, 1 May 1987 (1200 UTC) environments. Wind direction is according to standard compass. A half-barb equals 2.5 m s^{-1}; a full barb equals 5 m s^{-1}.

The relative flow profiles also demonstrate different characteristics among the three cases in the uppermost levels. Studies with the two-dimensional cloud model (Scala et al. 1990; Pickering et al. 1992) show that modification of updraft cores by the environmental wind field produces one of two types of anvil circulation: either an "overturning" (outflow directed mostly ahead of the LEC) or a "trailing" (outflow directed mostly to the rear of the LEC) structure. On the one extreme, weak front-to-rear flow at 15–16 km on 1 May (Fig. 14) is less inhibiting to the divergent upper-

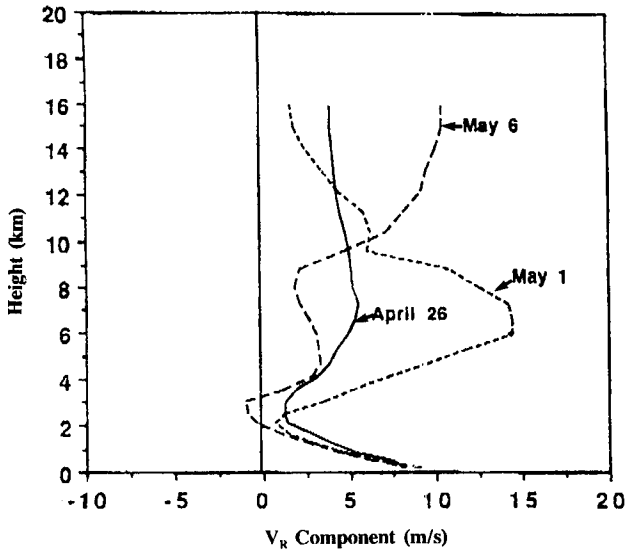

FIG. 14. Horizontal storm-relative flow $\mathbf{V}_R$ (m s^{-1}) calculated for the prestorm and LEC environments of the 26 April, 1 May, and 6 May ACSL.

level outflow. This causes the development of a forward anvil overhang. In the other case, the strong upper-level westerlies on 6 May suppress the forward spread of condensate and favor development of a trailing anvil structure.

As the different features observed in the relative flow fields for the 26 April, 1 May, and 6 May squall systems demonstrate, the gross structure and behavior of convective systems in the ACSL classification may be similar but variations in the finer aspects of the storm flow occur from storm to storm. These variations reflect both differences in the large-scale flow regime and sampling of the particular stage of the storm life cycle.

Figure 15 presents a conceptual model of the flow structure for a mature ACSL in a Lagrangian frame of reference. Storm-relative circulations are inferred from the flow fields shown in Figs. 13 and 14 and from the surface network calculations and two-dimensional model simulations. In Fig. 15, the thick arrows indicate the pathways of the major core updrafts and downdrafts that regenerate convective-scale transport and maintain the overall mesoscale structure of the system.

Mesoscale rear-to-front inflow feeds convective-scale downdrafts at the leading edge. These downdrafts, in turn, generate forced ascent into convective-scale updrafts. Strong inflow of dry, cold air into the front of this region mixes with and reduces the buoyancy of the convective updraft in midlevels. As a consequence, the updraft branch acquires a nearly horizontal tilt just above the freezing level and develops a front-to-rear flow of air directed into the trailing stratiform region. A second, weaker branch of the updraft forms in the middle and upper levels of the TSR. A similar double-updraft structure has been described by Roux et al. (1984) in their study of a West African squall line. Mixing between the forward updraft inflow and rear inflow branches is found near the freezing level (600 mb).

d. Thermodynamic processes in the trailing stratiform region

Composite profiles of θ_e in the prestorm and LEC are compared with composite profiles in the TSR for the 26 April, 1 May, and 6 May ACSLs (Fig. 16). The composite profiles are formed from three soundings at the triangle corners and two times of day constituting a suite of six soundings in each composite for each date.

The two prestorm composite profiles (26 April and 6 May) show a defined θ_e minimum near 339 K at 600 mb and 450 mb, respectively. The LEC composite sounding on 1 May shows no midtropospheric minimum in θ_e. The composite profiles of θ_e in the TSR all show a reduction or removal of the midtropospheric minimum in θ_e.

Comparison of the composite profiles in Fig. 16 shows that the Amazon systems affect the vertical distribution of equivalent potential temperature. These systems effectively remove or substantially reduce the midlevel tropospheric minimum in θ_e. This is accomplished by the upward transport of surface air containing high-θ_e values and release of latent heat in midlevels, and downward transport of cool, dry midtropospheric air. Evidence for midlevel warming is seen in the soundings shown in Fig. 10. The troposphere in the TSR of the 1 May system has been warmed nearly 2 K between 525 and 250 mb. An accompanying moistening of nearly 1 g kg^{-1} has also

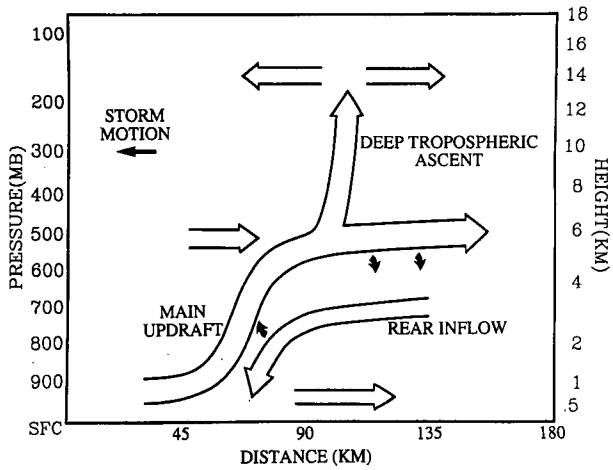

FIG. 15. Conceptual model of the flow structure for a mature ACSL constructed from a combination of vertical velocity and storm-relative flow calculations and two-dimensional cloud model simulations.

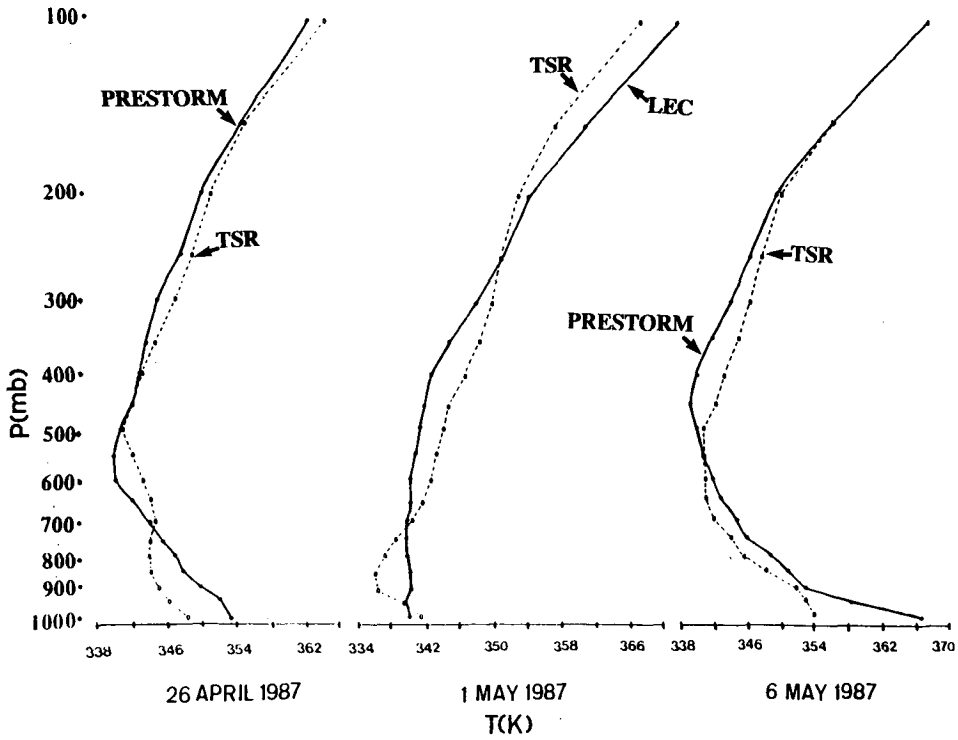

FIG. 16. Comparison of vertical profiles of θ_e derived for the triangle composite (three station) soundings for three ACSL: 26 April 1987 (1500 and 1800 UTC), 1 May 1987 (1200 and 1800 UTC), and 6 May 1987 (1500 and 1800 UTC).

occurred. Downward transport of dry (relatively low θ_e) air is also noted through the formation of a region of enhanced drying between 700 and 950 mb. This type of θ_e overturning was noted by Betts (1973) for Venezuelan squall lines. Fortune (1980) also showed that air in the wake of an African squall line had become "homogenized" through overturning of the θ_e profile. The stabilization of the vertical column in the TSR is noted in the θ_e profiles for each of the three Amazon cases and resembles the stabilization found in mesoscale anvils near Borneo by Johnson and Kriete (1982).

The vertical redistribution of θ_e suggests that the troposphere is well mixed by the ACSL. This finding, also concluded by Scala et al. (1990), implies that the Riehl and Simpson (1979) "hot tower" requirement for vertical transport may not be the only mechanism operating within organized convective systems over the Amazon Basin. While it is recognized that hot towers transport large quantities of sensible and latent heat, transport through protected hot tower conduits, if operating exclusively, would preserve the θ_e minimum in the wake of the deep convective region. Instead, the observed removal of the θ_e minimum and low-level decrease in θ_e imply that vertical motions in the ACSL might directly overturn the troposphere. Vertical transports of heat under these circumstances can be accomplished by mean upward and downward circulations ranging in scale from that of the ACSL to an integrated Hadley transport. The cores of the deep convective elements may in fact "leak" or actively detrain latent and sensible heats into their environment. Evidence for extensive detrainment was observed during aircraft flights into the ACSL, which found multiple layers of horizontal cloud extended from the flanks of the deep convection and outward from the rear of the deep convective towers. The entrainment of relatively dry midtropospheric air into the updraft cores, subsequent dilution of the cores, and detrainment of this air to the rear of the system provide a possible mechanism for the "leaking" process.

The importance of the trailing stratiform region to both the squall line total energy transport and to large-scale vertical energy transports in the global tropics will be presented in Part II.

4. Summary and conclusions

In this paper, we have examined the structure and dynamics of a distinct type of synoptic-scale convective system over the equatorial continental tropics, the Amazon coastal squall line (ACSL). ACSL are dis-

continuous lines of organized mesoscale cloud clusters that form along the northeastern coast of South America as sea-breeze-induced instability lines. The lines propagate across the central Amazon Basin at speeds of 50–60 km h^{-1}, with some maintaining enough coherence to arrive at the westernmost boundaries of the Amazon Basin 24–48 h later.

Analysis of satellite and rawinsonde data show that the ACSL undergo six possible stages in their life cycle: genesis, intensification, maturity, weakening, reintensification, and dissipation. Detailed analyses of surface PAM, satellite, radar, and aircraft observations also reveal that ACSL are composed of three distinct components: a prestorm region containing towering cumulus, LEC, and multiple precipitating layers of cloud in the TSR.

Calculations of divergence and vertical velocity for a mature ACSL indicate deep vertical ascent in the LEC and in a region of midlevel convergence in the TSR. The midlevel convergence is associated with a weak updraft above 500 mb and an unsaturated downdraft below. The vertical motions in the TSR are an order of magnitude smaller than those in the LEC. These findings are similar to the structure and dynamics of squall lines and other types of mesoscale convective systems in the tropics and midlatitudes (Houze 1989).

Storm motion, which is a consequence of a low-level to midlevel tropospheric wind maximum, produces a strongly sheared low-level inflow in all three of the ACSL cases examined. This shear may play an important role in the longevity of the storm system. Strong inflow of cold, dry midtropospheric air into the deep convective cloud elements reduces the buoyancy of updraft cores and causes the updraft branch of the circulation to tilt strongly rearward just above the freezing level. A second, weaker branch of updraft forms in the middle and upper levels of the trailing stratiform region.

Composite profiles of θ_e for prestorm, LEC, and TSR of three ACSL, show important thermodynamic transformations produced by storm-scale circulations. The ACSL stabilize the troposphere in their wake and remove the tropospheric minimum in θ_e. We hypothesize that the removal of the θ_e minimum is accomplished through direct mixing by means of vertical motions in the storm and through detrainment in multiple layers in the midtroposphere in the wake of the squall system. Our evidence supports the contention that energy transport through protected hot towers is not the only mechanism that accomplishes the required vertical transports over the Amazon Basin during the wet season. Energy budgets and transports associated with the ACSL will be the main focus for Part II of our study.

Acknowledgments. We gratefully acknowledge the sustained support provided by the Tropospheric Chemistry Program of NASA. This support, following the field work in ABLE 2A and 2B, has made analysis of extensive and unique datasets possible.

A large part of this paper is drawn from Harold L. Massie's doctoral dissertation and from the doctoral research of Jeffrey Halverson.

REFERENCES

Barnes, G. M., and K. Sieckman, 1984: The environment of fast- and slow-moving tropical mesoscale convective cloud lines. *Mon. Wea. Rev.*, **112**, 1782–1794.

Betts, A. K., 1973: Non-precipitating cumulus convection and its parameterization. *Quart. J. Roy. Meteor. Soc.*, **99**, 178–196.

——, R. W. Grover, and M. W. Moncrieff, 1976: Structure and motion of tropical squall-lines over Venezuela. *Quart. J. Roy. Meteor. Soc.*, **102**, 395–404.

Carlson, D. C., 1981: Weather satellite interpretation—Introduction to satellite imagery. NOAA Tech. Memo. NWS SR-103, 47 pp.

Chalon, J. P., G. Jaubert, F. Roux, and J. P. Lafore, 1988: The West African squall line observed on 23 June 1981 during COPT81: Mesoscale structure and transports. *J. Atmos. Sci.*, **45**, 2744–2763.

Chong, M., P. Amayenc, G. Scialom, and J. Testud, 1987: A tropical squall line observed during the COPT81 experiment in West Africa. Part I: Kinematic structure inferred from dual Doppler radar data. *Mon. Wea. Rev.*, **115**, 671–694.

Cohen, J. C. P., C. A. Nobre, and M. A. F. da Silva Dias, 1989: Mean distribution and characteristics of the squall lines observed over the Amazon Basin. *Third Int. Conf. on Southern Hemisphere Meteorology and Oceanography,* Buenos Aires, Argentina, 205–207.

Davis, J. C., 1986: *Statistics and Data Analysis in Geology.* John Wiley and Sons, 646 pp.

Fortune, M., 1980: Properties of African squall lines inferred from time-lapse satellite photography. *Mon. Wea. Rev.*, **108**, 153–168.

Frank, W. M., 1978: The life cycles of GATE convective systems. *J. Atmos. Sci.*, **35**, 1256–1264.

——, and J. L. McBride, 1989: The vertical distribution of heating in AMEX and GATE cloud clusters. *J. Atmos. Sci.*, **46**, 3464–3478.

Gallus, W. A., Jr., and R. H. Johnson, 1991: Heat and moisture budgets of an intense mid-latitude squall line. *J. Atmos. Sci.*, **48**, 122–146.

Gamache, J. F., and R. A. Houze, Jr., 1982: Mesoscale air motions associated with a tropical squall line. *J. Atmos. Sci.*, **110**, 118–135.

Garstang, M., S. Ulanski, S. Greco, J. Scala, R. Swap, D. Fitzjarrald, D. Martin, E. Browell, M. Shipham, V. Connors, R. Harriss, and R. Talbot, 1990: The Amazon Boundary Layer Experiment (ABLE 2B): A meteorological perspective. *Bull. Amer. Meteor. Soc.*, **71**, 19–32.

Greco, S., R. Swap, M. Garstang, S. Ulanski, M. Shipham, R. C. Harriss, R. Talbot, M. O. Andreae, and P. Artaxo, 1990: Rainfall and surface kinematic conditions over central Amazonia during ABLE 2B. *J. Geophys. Res.*, **93**, 17 001–17 014.

Haltiner, G. J., and F. L. Martin, 1957: *Dynamical and Physical Meteorology.* McGraw-Hill, 470 pp.

Harriss, R. C., M. Garstang, S. C. Wofsy, S. M. Beck, R. J. Bendura, J. R. B. Coelho, J. W. Drewry, J. M. Hoell, P. A. Matson, R. J. McNeal, L. C. B. Molion, R. L. Navarro, V. Rabine, and R. L. Snell, 1990: The Amazon Boundary Layer Experiment: Wet season 1987. *J. Geophys. Res.*, **93**, 16 721–16 736.

Houze, R. A., 1977: Structure and dynamics of a tropical squall line system. *Mon. Wea. Rev.*, **105**, 1540–1567.

——, 1989: Observed structure of mesoscale convective systems and implications for large-scale heating. *Quart. J. Roy. Meteor. Soc.*, **115**, 425–461.

Johnson, R. H., and D. L. Priegnitz, 1981: Winter monsoon convection in the vicinity of North Borneo. Part II: Effects on large-scale fields. *Mon. Wea. Rev.*, **109**, 1615–1628.

——, and D. C. Kriete, 1982: Thermodynamic and circulation characteristics of winter monsoon tropical mesoscale convection. *Mon. Wea. Rev.*, **110**, 1898–1911.

Kousky, V. E., 1980: Diurnal rainfall variation in northeast Brazil. *Mon. Wea. Rev.*, **108**, 488–498.

——, and L. C. B. Molion, 1981: Una contribucao a climatologia dinamica da troposfera sobre a Amazônia. INPE-2030-RPI/050, Sao Jose dos Campos, S.P. Brazil.

Leary, C. A., and R. A. Houze, Jr., 1979: The structure and evolution of convection in a tropical cloud cluster. *J. Atmos. Sci.*, **36**, 437–457.

Molion, L. C. B., 1987: On the dynamic climatology of the Amazon Basin and associated rain-producing mechanisms. *The Geophysiology of Amazonia: Vegetation and Climate Interactions*, R. Dickerson, Ed., Wiley Interscience, 391–407.

O'Brien, J. J., 1970: Alternative solutions to the classical vertical velocity problem. *J. Appl. Meteor.*, **9**, 197–203.

Ogura, Y., and M.-T. Liou, 1980: The structure of a midlatitude squall line: A case study. *J. Atmos. Sci.*, **37**, 553–567.

Pickering, K. E., A. M. Thompson, J. R. Scala, W.-K. Tao, J. Simpson, and M. Garstang, 1991: Photochemical ozone production in tropical squall line convection during NASA/GTE/ABLE 2A. *J. Geophys. Res.*, **96**, 3099–3114.

——, ——, ——, ——, R. R. Dickerson, and J. Simpson, 1992: Free tropospheric ozone production following entrainment of urban plumes into deep convection. *J. Geophys. Res.*, **97**, 17 985–18 000.

Riehl, H., and J. Simpson, 1979: The heat balance in the equatorial trough zone, revisited. *Contrib. Atmos. Phys.*, **52**, 287–305.

Rotunno, R., J. B. Klemp, and M. L. Weisman, 1988: A theory for strong, long-lived squall lines. *J. Atmos. Sci.*, **45**, 463–484.

Roux, F., J. Testud, M. Payen, and B. Pinty, 1984: West African squall-line thermodynamic structure retrieved from dual-Doppler radar observations. *J. Atmos. Sci.*, **41**, 3104–3121.

Scala, J. R., M. Garstang, W.-K. Tao, K. F. Pickering, A. M. Thompson, J. Simpson, V. W. J. H. Kirchhoff, E. V. Browell, G. W. Sachse, A. L. Torres, G. L. Gregory, R. A. Rasmussen, and M. A. K. Khalil, 1990: Cloud draft structure and trace gas transport. *J. Geophys. Res.*, **95**, 17 015–17 030.

Silva Dias, M. A. F., and R. N. Ferreira, 1992: Application of a linear spectral model to the study of Amazonian squall lines during GTE/ABLE 2B. *J. Geophys. Res.*, **97**, 20 405–20 419.

Simpson, J., and W.-K. Tao, 1993: Goddard cumulus ensemble model. Part II: Applications for studying cloud precipitating processes and for NASA TRMM. *Terr., Atmos. Oceanic Sci.*, **4**, 35–72.

Smull, B. F., and R. A. Houze, Jr., 1987: Rear inflow in squall lines with trailing stratiform precipitation. *Mon. Wea. Rev.*, **115**, 2869–2889.

Soong, S.-T., and Y. Ogura, 1980: Response of trade-wind cumuli to large-scale processes. *J. Atmos. Sci.*, **37**, 2035–2050.

——, and W.-K. Tao, 1980: Response of deep tropical clouds to mesoscale processes. *J. Atmos. Sci.*, **37**, 2016–2034.

——, and ——, 1986: The study of the response of deep tropical clouds to mesoscale processes: Three-dimensional numerical experiments. *J. Atmos. Sci.*, **43**, 2653–2676.

Tao, W.-K., and J. Simpson, 1989: Modeling study of a tropical squall-type convective line. *J. Atmos. Sci.*, **46**, 177–202.

——, and ——, 1993: Goddard cumulus ensemble model. Part I: Model description. *Terr., Atmos. Oceanic Sci.*, **4**, 73–116.

——, ——, and S.-T. Soong, 1991: Numerical simulation of a subtropical squall line over Taiwan Straits. *Mon. Wea. Rev.*, **119**, 2699–2723.

Thorpe, A. J., M. J. Miller, and M. W. Moncrieff, 1982: Two-dimensional convection in nonconstant shear: A model of midlatitude squall lines. *Quart. J. Roy. Meteor. Soc.*, **108**, 739–762.

Zipser, E. J., 1977: Mesoscale and convective-scale downdrafts as distinct components of squall-line structure. *Mon. Wea. Rev.*, **105**, 1568–1589.